J. Fluid Mech. (2006), *vol.* 556, *pp.* 253–269. © 2006 Cambridge University Press
doi:10.1017/S0022112006009542 Printed in the United Kingdom

Granular flow transitions on sinusoidal surfaces

By CARLOS E. CAICEDO-CARVAJAL[1], BENJAMIN J. GLASSER[2] AND TROY SHINBROT[1]

[1]Department of Biomedical Engineering, Rutgers University, Piscataway, NJ 08855, USA

[2]Department of Chemical and Biochemical Engineering, Rutgers University, Piscataway, NJ 08855, USA

(Received 22 November 2004 and in revised form 29 November 2005)

We report on a newly discovered bifurcation that occurs in dry grains flowing down a chute with a wavy bottom. We find that the bifurcation outwardly resembles the long-known fluid analogue of inviscid channel flow over a wavy bottom reported in 1886 by Lord Kelvin; however, in detail, the two situations differ significantly. We compare three distinct states seen in the granular system: a 'regular' flow in phase with the bottom wave; an 'antiregular' flow that is out of phase; and a 'flat' flow in which the surface slides nearly uniformly downhill. Additionally, we discuss evidence that sustained subsurface circulation in the granular bed, accompanied by strong fluctuations in flow velocities, can appear in granular flows over wavy surfaces.

1. Background

Over a century ago, Lord Kelvin predicted a surface wave bifurcation for fluid flow through a channel with a wavy bottom (Thomson 1886; Lamb 1932). This bifurcation defines a transition between 'regular' flow, in which the surface is in phase with the wavy bottom, and 'antiregular' flow, in which it is out of phase. Since that time, experimental and computational studies have investigated the behaviour of fluid flow over wavy surfaces (Krettenauer & Schumann 1992; Gong, Taylor & Dornbrack 1996; Hudson, Dykhno & Hanratty 1996; Nakayama & Sakio 2002; Günther & Rohr 2003), shear in this geometry (Benjamin 1958), and mechanisms of wave generation in two-phase wavy flows (Montalbano & McCready 1998). Although the observations made by Lord Kelvin for fluids have stood for a century, no studies to our knowledge have investigated similar transitions in granular flow on wavy bottoms. Yet the precise problem of granular flow over wavy and rough bottoms is encountered in both laboratory (Takahashi 1981; Savage & Hutter 1989; Iverson 1997; Pouliquen 1999; Hanes & Walton 2000; Denlinger & Iverson 2001; Louge 2003) and geophysical debris (Hakonardottir *et al.* 2003; Iverson 1997) flows, and there are theoretical suggestions from simulations of single balls bouncing down a bumpy incline (Dippel, Bartrouni & Wolf 1996) that such transitions may occur as well. In this paper, we perform, to the best of our knowledge, the first experimental investigations of this problem, and we find that there is indeed a sharp transition between regular and antiregular granular flow as the angle of the wavy chute is varied. The granular transition differs in important ways from the fluid one, and we propose a mechanism involving circulatory subsurface flows that seems to capture some of the essential kinetics involved.

Studies of shear in granular materials date back at least to Bagnold's pioneering work on desert sand transport (Bagnold 1936), with related geophysical reports

https://doi.org/10.1017/S0022112006009542 Published online by Cambridge University Press

appearing many years before that (Bishop 1713; Lyell 1858; Hopkins 1862). More recently, work on shear in well-instrumented cells (Rabinowicz 1956; Miller, O'Hern 1996; Menon & Durian 1997; Howell & Behringer 1999; Losert *et al.* 2000; Mueth *et al.* 2000), chutes (Savage & Hutter 1989; Hanes & Walton 2000; Forterre & Pouliquen 2001; Goldfarb, Glasser & Shinbrot 2002; Gray, Tai & Noelle 2003; Louge 2003) and other systems (Hsiau & Hunt 1993; Komatsu *et al.* 2001) has attempted to clarify the mechanisms of granular response to controlled stresses. Notwithstanding these investigations, granular beds often display solid-like and fluid-like qualities side-by-side within a single experiment, and generally applicable rules underlying granular phenomena remain elusive (several comprehensive surveys are available from a variety of perspectives e.g. Bridgwater 1976; Savage *et al.* 1983; Jenkins 1986; Johnson, Natt & Jackson 1990; Jaeger, Nagel & Behringer 1996; Iverson 1997; Goddard & Alam 1999; Kadanoff 1999). We know that these behaviours have important practical ramifications. On the laboratory scale, periodic disturbances of granular tumbling flows have been shown to result in improvements in mixing rates by orders of magnitude (Shinbrot, Alexander & Muzzio 1999), and in a provocative example on geophysical scales, a periodic array of stone barriers have recently been erected to dissipate the destructive force of snow avalanches in the town of Neskaupstadur in eastern Iceland (Hakonardottir *et al.* 2003; Johannesson & Hakonardottir 2003). Moreover, recent hydrodynamic treatments (Gray *et al.* 2003) have shown great promise in chute flows. In the present paper, we seek to advance the understanding of granular transitions in flows across wavy bottoms: a topic whose understanding lags considerably behind that in the seemingly closely related field of fluid dynamics (Hewgill, Reeder & Shinbrot 1981; Bocquet, Errami & Lubensky 2002; Hakonardottir *et al.* 2003; Johannesson & Hakonardottir 2003; Silbert *et al.* 2003).

2. Phenomenology

As we have emphasized, fluid flows over wavy surfaces have been studied for many years, both as paradigmatic theoretical problems and because practical systems are seldom uniform (Iverson 1997). One such system appears in channel flow across a wavy surface, as shown in figure 1 from a fluids experiment in our laboratory. In fluids experiments, channel flow undergoes a hysteretic bifurcation from the 'regular' state at higher flow rates (figure 1*a*) where the fluid free surface is in phase with the (sinusoidal) channel bottom to the 'antiregular' state at lower flow rates (figure 1*b*), where the free surface is out of phase with the channel bottom. This bifurcation coincides with two dynamical features of interest: the first is the emergence of a hydraulic jump (Stoker 1957) (indicated in figure 1*c*), the second is the creation of a recirculation loop (also indicated) just downstream of the jump. This bifurcation is very robust, and persists despite being removed from the ideal potential-flow limit of vanishing viscosity (our Reynolds number is $\sim$100).

To investigate a granular analogue of this bifurcation, we construct a 244 cm long, 10.2 cm wide chute in which we fit a variety of amplitude and wavelength sinusoidal bottoms. Chutes notoriously tribo-charge as dissimilar materials rub across the chute surface (Shinbrot 1985), so the bottoms (which are cut into sinusoidal shapes from wood slats) are covered with smooth grounded aluminium flashing to provide a reproducible and minimally charged surface on which to perform experiments. The sides of the chute are clear acrylic to permit us to see near-wall flows, and to further limit charging, we apply antistatic fluid to these sides before each experimental trial. In figure 2, we display characteristic results, here for a sinusoidal bottom with wavelength

https://doi.org/10.1017/S0022112006009542 Published online by Cambridge University Press

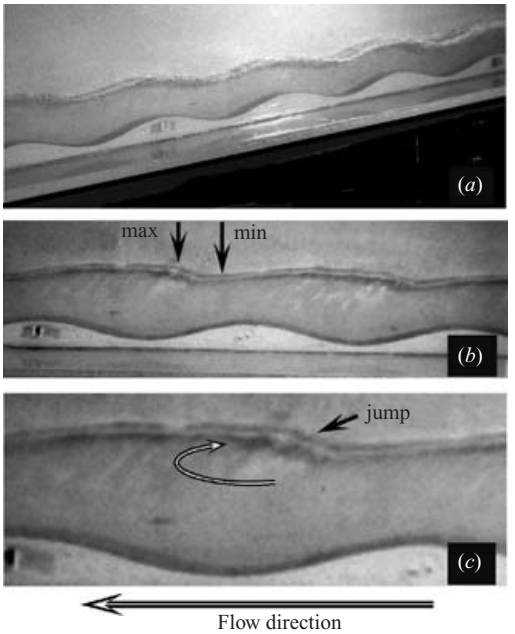


FIGURE 1. Snapshots of steady (*a*) 'regular' flow and (*b*) 'antiregular' flow of water in a horizontal channel with a sinusoidal bottom. As indicated in (*b*), in the antiregular state, the maximum of the free surface is over the minimum of the channel bottom. (*c*) Enlarged view of antiregular flow showing hydraulic jump. The channel is 5 cm wide, 244 cm long and is fed from the right; the wavelength and peak-to-peak amplitude of the sinusoidal insert are 30 cm and 2.5 cm, respectively.

20 cm and peak-to-peak amplitude 2 cm. Art sand (coloured irregular glass grains of mean diameter 0.5 mm) is released onto the chute from an upstream hopper whose outlet is 10 cm above the chute surface, and whose mass flow rate is measured over a period of minutes to remain stable at $281 \pm 2\,\mathrm{g\,s^{-1}}$.

From this figure, we see that there is, indeed, a transition from regular (figure 2*a*) to antiregular (figure 2*b*) flow, here as the angle of incline of the chute is reduced from 32.7° to 31.2° as measured with a digital level. As with the fluid case, there appears to be an identifiable minimum (indicated in figure 2*b*) in the antiregular state, possibly accompanied by an upstream hydraulic jump. The minimum and nearby maximum are identified in the enlarged side view of figure 2(*c*). In the latter figure, we also use two differently coloured, but otherwise identical, grains to study transport; this is discussed in a later section.

3. Transients and final states

We performed several independent experiments to evaluate the dependencies of the granular form of this surface-wave bifurcation. First, we measured the length of time, τ, taken to achieve a steady final state as a function of chute inclination angle, ϑ. To make our measurements reproducible, we opened the hopper onto a clean chute at a fixed inclination angle, and evaluated the time taken until the central 6 wavelengths (excluding one wavelength at the top and one at the bottom where there are some variations due to end effects) of the chute all exhibited the same state.

https://doi.org/10.1017/S0022112006009542 Published online by Cambridge University Press

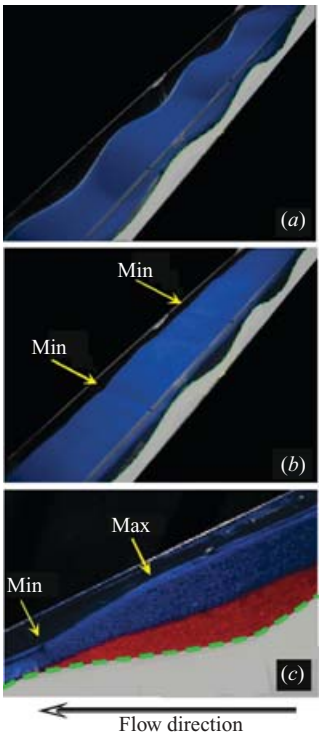


FIGURE 2. Snapshots of (*a*) 'regular' flow (at 32.7° chute inclination) and (*b*) 'antiregular' flow (at 31.2° inclination) of dry sand in a tilted channel with a sinusoidal bottom. As indicated in (*b*)–(*c*), the peak of the free surface is over the trough of the channel bottom in the antiregular state. (*c*) Enlarged view of antiregular flow, showing that a portion of the bed that was released earlier (red) is eroded more slowly than flowing grains released subsequently (blue), which travel mostly near the surface. There appears to be a hydraulic jump between the 'min' and the 'max' arrows in (*c*) (see text). The channel is fed from a hopper to the right of the photographs. The sinusoidal bottom is identified by the dashed green line.

Flow states in the wavy chute are significantly hysteretic; however, the sequence of events that typically occurs after opening the hopper is as follows. When the hopper is first opened, grains relax to fill the valleys of the chute. A snapshot showing this process while it is occurring is shown in the inset in figure 3(*a*). In this snapshot, grains flowing from uphill (to the right) cascade in a jet (cf. Hakonardottir *et al.* 2003) over the top of an upstream sinusoidal peak to impinge on the downstream end of the next peak (black arrowheads). The formation of a jet occurs when the inlet kinetic energy of the flowing grains is very high (as occurs when the inlet hopper is raised); if the kinetic energy is lower, the grains initially cover the entire chute in a uniform blanket that gradually thickens in the troughs until the final state is reached. In the case where a jet appears, grains in the jet fly nearly ballistically over the underlying bed. When these grains collide with the downstream surface, they lose kinetic energy and subsequently collapse into the nearest valley. During this collapse, the front of the jet (indicated by arrowheads in the inset) moves downhill until the upstream valley is filled with debris from prior collisions with the downstream surface.

At this point (which is reached either with an initial jet, or for less energetic inlet speeds without the jet) one of three steady states emerge, depending on the chute inclination. If the chute inclination is greater than about $\vartheta_{c1} = 32.3°$, the static grains

https://doi.org/10.1017/S0022112006009542 Published online by Cambridge University Press

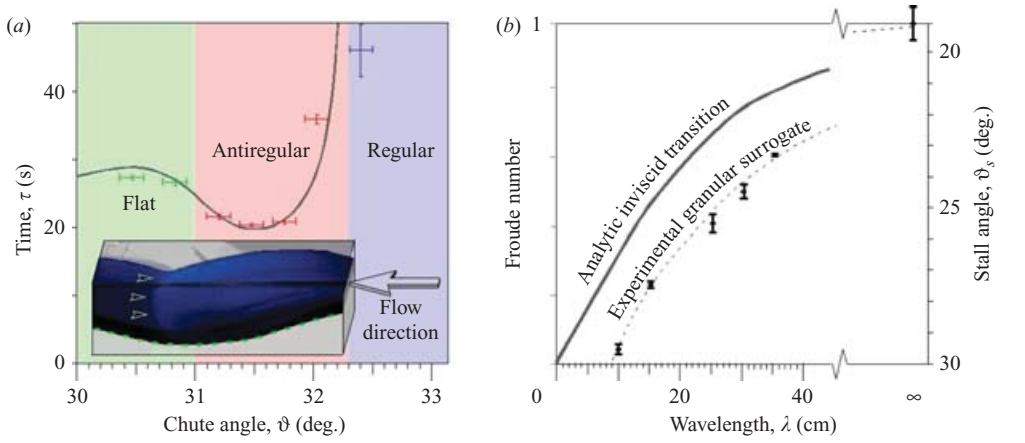


FIGURE 3. (*a*) Time to reach steady state *vs.* chute angle. The data points are averaged over 10 separate trials. Angles greater than about 32.5° attain the regular state almost immediately. Coloured regions indicate flat, antiregular and regular regimes described in text; boundaries between these regimes are precise in our experiment, but change with grain properties and environmental conditions and should therefore be treated as approximate. The inset shows a snapshot of the evolving flow in an antiregular state (see text). (*b*) Plots of fluid (solid line) and granular (dashed) transitions between regular and antiregular flow *vs.* wavelength λ of sinusoidal bottom. For the fluid case, we plot $Fr = \tanh(kd)/kd$, where d is the depth of the flow, taken to be 5 cm, and k is the wavenumber, $2\pi/\lambda$. For the granular case, higher kinetic energy flows stall at lower chute angle (see text), so for comparison we plot decreasing stall angle (right-hand ordinate) alongside increasing Froude number (left-hand). Note that because the scales are different, any agreement is at most qualitative.

in the valley are washed downstream by the continuing influx of grains flowing downhill, to leave a regular surface. If the inclination is below this value, a more complex flow is produced, in which the surface flows downhill but, as we demonstrate shortly, subsurface flows recirculate (Gray *et al.* 2003) to produce the surface minima shown in figure 2(*b*). Finally, if the chute inclination is below about $\vartheta_{c2} = 31°$, the valleys fill completely to produce a flat static bed at the height of the sinusoidal peaks, and inflowing grains slide with nearly uniform depth and speed on this bed.

Corresponding to each of these states is a time, τ, required to reach the final state, as we defined previously. In the main part of figure 3(*a*), we plot measurements of τ at chute angles in the range 30°–33°. Each measurement is an average over 10 separate experimental trials. Close to the transition angle of about $\vartheta_{c1} = 32.3°$, the surface invariably starts out in a regular in-phase state. Slightly below ϑ_{c1}, the most downstream valley fills with grains, after which the surface in that valley slowly transitions to an antiregular state. This appears to cause grains in the next valley upstream to slow; that valley then becomes antiregular as well, and so forth up the chute. The regular–antiregular transition appears to display significant critical slowing down (Howell & Behringer 1999): as the chute angle becomes closer to ϑ_{c1}, the flow takes increasingly longer to settle into the final state reported. By contrast, the transition between antiregular and flat surface flows around $\vartheta_{c2} = 31°$ seems to be continuous.

To aid the eye, we have correspondingly plotted in grey the function indicated in the figure containing a tanh to fit the transition at ϑ_{c1}, and a square-root singularity to fit the apparent slowing down (explicitly, the curve shown is: $\tau = [2 - \tanh(2(\vartheta - \vartheta_{c1}))]/2\sqrt{|\vartheta - \vartheta_{c2}|}$). We stress that this is not a theoretical

https://doi.org/10.1017/S0022112006009542 Published online by Cambridge University Press

model; the constants are chosen strictly for convenience, and we present this function only as a curve fit that seems to define roughly the experimental phenomenology that we observe, i.e. one smooth continuous transition at ϑ_{c1} followed by a second showing slowing-down at around ϑ_{c2}. We compare these phenomenological descriptions with other data shortly.

4. Parametric dependence

In a second set of experiments, we varied the wavelength of the sinusoidal chute bottom. We additionally investigated doubling the amplitude of the sinusoidal chute shape; however, this had the effect of stalling all motion in the chute valleys, which in turn eliminated the antiregular state. We therefore kept the amplitude at the lower value of 2 cm peak-to-peak and varied the sinusoidal wavelength. Results from these experiments are shown in figure 3(*b*). Here, we fabricated several sinusoidal inserts with wavelengths ranging from 10 to 40 cm. For a given wavelength insert, we maintained a constant inflow rate ($281 \pm 2\,\mathrm{g\,s^{-1}}$ as before), and beginning at a steep angle, we slowly decreased the chute angle until the flow stalled. For each of the wavelengths shown, the surface went through a regular, antiregular and flat state as indicated in figure 3(*a*). These transitions are somewhat variable, as indicated by the error bars in figure 3(*a*). By comparison, the stall angle, ϑ_s seemed to be more reproducible and represents a fixed upper bound on the other transitions, so we measured ϑ_s which is shown in figure 3(*b*) as a surrogate for the other transitions. Each data point here is the average of 5 experimental trials at the specified wavelength. The dashed curve through the data is an exponential fit that asymptotes to the flat chute value of about 19° (appropriate to our chute and grains) as the wavelength $\to \infty$.

Also in this plot, we include a curve (solid line) of the Froude number as a function of wavelength predicted from Kelvin's analysis of an inviscid and irrotational fluid. For fluid flow over a wavy bottom, the Froude number is defined in the usual way as a ratio of kinetic to potential energies:

$$Fr_f = \frac{v^2}{2gd}, \tag{1}$$

where v is the mean surface velocity of the fluid, g is gravity, and d is the characteristic depth of the flow. Kelvin (Thomson 1886; Lamb 1932) described a transition between regular and antiregular flow at the critical Fr:

$$Fr_f^* = \frac{\tanh(kd)}{kd}, \tag{2}$$

for a sinusoidal bottom of wavenumber k. To provide a comparable hydrodynamic treatment of our chute flow, we must define relevant kinetic and potential energies (Gray *et al.* 2003). The kinetic energy per unit mass of grains can be established directly from measurements of the granular inflow, as described below. The relevant potential energy is not entirely unambiguous, however, since any of several length scales could be used to calculate it. Prior work on granular flow down inclines has shown that the maximum slope controls the speed of the flow (Savage & Hutter 1989; Hanes & Waltor 2000; Louge 2003); this slope is closely approximated in our system by $h\sin(\vartheta)/\lambda$, where h is the depth of thes inusoidal bottom, λ is its wavelength, and ϑ is the angle of inclination of the chute. The vertical length scale that is most germane to calculating the potential energy is thus approximately $h\sin(\vartheta)$, and so we

https://doi.org/10.1017/S0022112006009542 Published online by Cambridge University Press

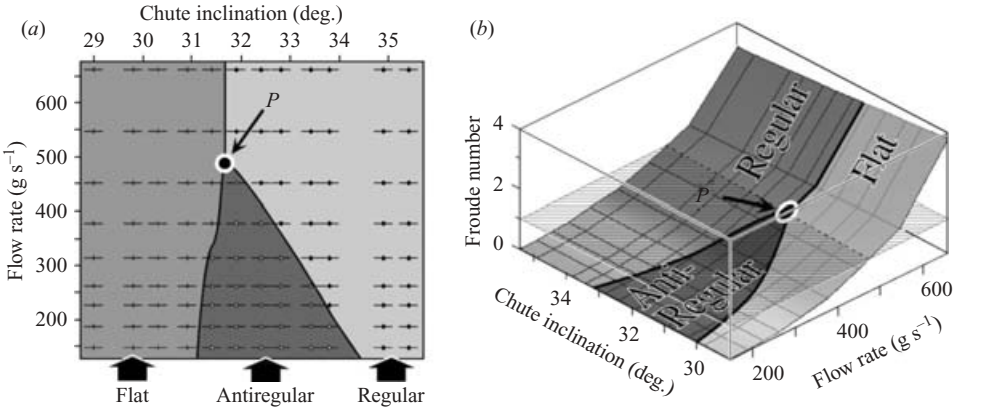


FIGURE 4. Phase diagram, showing the effect of inflow rate onto the chute and chute inclination on the flow state. (*a*) Data are shown for 9 values of flow rate and 12 values of inclination, and error bars are as shown. The transition lines are approximate; the state changes at the nearest datum on either side of the lines. (*b*) For the same flow rates and inclinations, we plot the Froude number calculated using equation (3), and we superimpose the transition curves from (*a*). We also show a hatched plane at $Fr = 1$; above $Fr = 1$, hydraulic jumps cannot be sustained, and the antiregular state (which contains a hydraulic jump, cf. figure 2*c*) disappears.

define the Froude number for the wavy granular flow to be:

$$Fr_s = \frac{(Q/\rho A)^2}{2gh \sin \vartheta}. \tag{3}$$

Here, Q and A are, respectively, the measured mass flow rate and orifice area at the inlet to the chute, ρ is the density (which we hold to be the bulk density of our glass beads, 2.5 g cm^{-3}), and g is gravity.

The chute angle, ϑ, appears in the denominator, and so Fr increases as ϑ decreases. Correspondingly, in figure 3(*b*), we plot Kelvin's analytic curve for fluids for increasing critical Froude number (left-hand ordinate), alongside our data obtained for grains for decreasing stall angles (right-hand ordinate). As we have stressed, the stall angle is a convenient and reproducible surrogate for the other transitions seen, and does not in closed form predict the critical Froude number. Nevertheless, figure 3(*b*) indicates that despite obvious differences between the simplified inviscid and irrotational fluid model and the strongly dissipative (Goldhirsch & Zanetti 1993; Du, Li & Kadanoff 1995; Henrique *et al.* 1998) (and as we will show, significantly circulatory) experimental granular flow, transitions in both cases tend toward higher kinetic energy at longer wavelength.

4.1. *Phase diagrams*

To explore more fully the parametric dependencies of the flow transitions in the wavy chute, we also varied the incoming flow rate to the chute. For this purpose, we used a wavy chute of fixed wavelength, 20 cm, and peak-to-peak amplitude, 2 cm, and we investigated 108 parameter sets consisting of 12 chute inclinations and 9 flow rates. Flow rates were set by inserting plates with fixed diameter orifices at the end of the inlet hopper; for each orifice size, we measured the flow rate as before, and in figure 4(*a*), we display how the flow state depends on inclination and flow rate.

The state of the flow was established in two ways. First, we determined by visual inspection whether the free surface was in phase with the sinusoidal bottom (for

https://doi.org/10.1017/S0022112006009542 Published online by Cambridge University Press

regular flow) and, if not, whether the surface had a minimum (for antiregular flow) or not (for flat flow). Secondly, we measured the volume of grains (the 'hold-up') contained in each cycle of the sinusoidal chute, which we found to be a signature of the state that correlates strongly with visual observations. For the flat state, the hold-up is 440 ± 20 ml; for the antiregular state the hold-up is 390 ± 20 ml; and for the regular state, the hold-up varies between 50 ml and 150 ml, depending on flow rate. The uncertainties are estimates based on the accuracy of measuring flow heights (and so the hold-up) through the transparent sidewall of the chute.

From figure 4(a), we see that distinct flat, antiregular and regular states appear for low flow rates, but at flow rates above about $500\,\mathrm{g\,s^{-1}}$ (point P in the figure), the antiregular state vanishes and the flow undergoes a transition between a flat state, at low chute angles, and a regular state, at higher angles.

By comparison, in figure 4(b), we plot the Froude number calculated using (3) as the chute inclination and flow rate are varied. Also in figure 4(b), we plot the plane $Fr_s = 1$ and we superimpose the states from figure 4(a). Apparently the antiregular state disappears above point P, i.e. above about $Fr_s = 1$. The disappearance of the antiregular state, which contains a hydraulic jump as shown in figure 2(b), is to be expected above $Fr = 1$, where hydraulic jumps cannot be sustained. The source of the λ-shaped antiregular boundary in figure 4(a, b) is not so readily explained, however.

5. Velocimetry

We therefore seek to unveil the mechanism underlying the granular transition in greater detail. For this purpose, we have performed particle image velocimetry (PIV) (Wightman *et al.* 1995), evaluating surface particle velocities in the three states indicated in figure 3(a). These data, discussed next, confirm that the flat, antiregular and regular states are indeed distinct, and are signatures of very different internal mechanisms of energy dissipation in the granular flow that are not captured well by averaged measures such as the Froude number. Results of these experiments are shown in figure 5 for PIV taken from above in each of the three flow states. In each plot, we show in grey the location of the sinusoidal trough beneath. Velocity fields are averaged over 2 s (1000 high-speed video frames) in each case.

These velocimetry data provide several notable findings. First, the regular state exhibits an increase in speed at the upstream aspect of the trough ($2.8\,\mathrm{m\,s^{-1}}$ average as indicated), and a decrease at the downstream aspect ($1.1\,\mathrm{m\,s^{-1}}$). This is as expected: in the regular state, grains follow the contour of the underlying chute (cf. figure 1a), and accelerate in the regions of steepest gradient and slow as the gradient decreases. The flow is qualitatively different in the antiregular state: here as shown in figure 2(b), the flow is thin – and rapid – near the crests of the underlying chute, and is thicker – and slower – in the troughs. The surface flow throughout the trough region is both more uniform and substantially slower (between 0.1 and $0.5\,\mathrm{m\,s^{-1}}$) than in the regular case, and flow actually accelerates (to about $0.5\,\mathrm{m\,s^{-1}}$) above the crest of the sinusiodal insert.

Second, as indicated by sample numerical data above each plot in figure 5, quantitative surface speeds are reduced by about an order of magnitude in the antiregular state as compared to the regular state. Since mass flow rates are held constant, this implies that the flowing layer must be an order of magnitude thicker in the antiregular state than in the regular.

Finally, the flat state is measured to be essentially independent of location, and by all appearances seems to consist of a slowly and uniformly sliding layer on a

https://doi.org/10.1017/S0022112006009542 Published online by Cambridge University Press

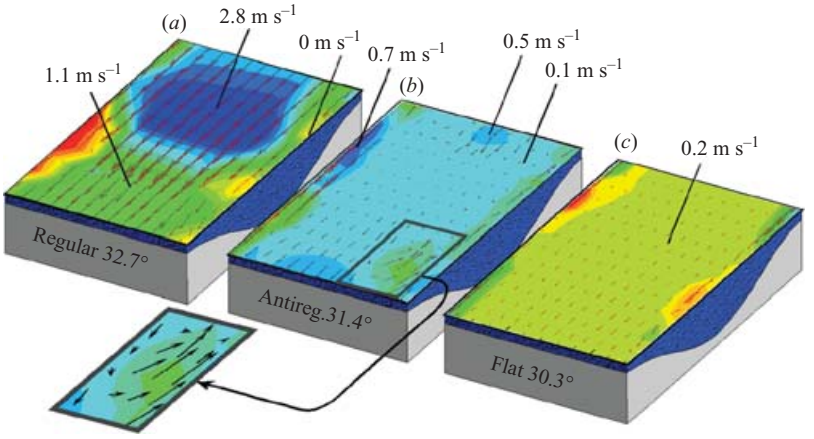


FIGURE 5. Surface velocity fields, averaged over 1000 frames, during (*a*) regular, (*b*) antiregular and (*c*) flat flows. In the regular case, there are no surprises: flow is rapid and accelerates upstream of valleys and slows downstream. At the other extreme in the flat case, flow is an order of magnitude slower, and, since valleys are filled with stalled grains, is very uniform. In the intermediate antiregular state, surface flow speeds are locally variable, and sometimes even display circulatory eddies as in the enlarged inset. Note from the identified speeds that colour scales differ in the three cases.

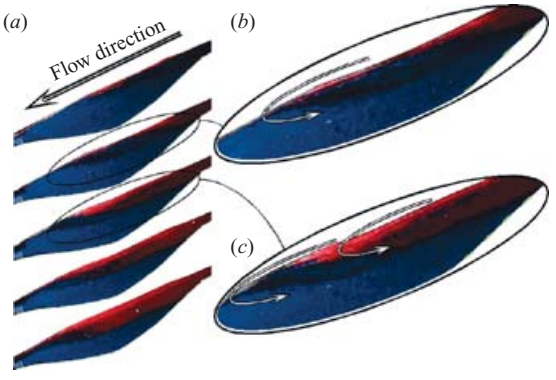


FIGURE 6. (*a*) Snapshots of the trough through the transparent sidewall of the chute at the third trough from the top during antiregular flow in a two-colour sand experiment. The sequence of flow is shown from top to bottom as time progresses. There is an intermittent behaviour in the penetration of blue sand into the initially flowing red sand. Enlarged views shown in (*b*) and (*c*) suggest subduction of the red sand in multiple recirculation loops, indicated by arrows.

flat stationary bed that is formed when the sinusoidal troughs fill with static grains. Noting again that the mass flow rate is held fixed in all three cases, we can use the flat state to serve as a point of reference for the regular and antiregular states. That is, the regular steady flow must be much thinner than the flat state in order to conserve mass, and by the same token in the antiregular state, the surface height is nearly identical to that in the flat state, so the spatially averaged flow speed must be the same in the two states, i.e. about 0.2 m s^{-1}. Since most of the surface flow above the crest in the antiregular state is at a lower speed (about 0.1 m s^{-1} as indicated), it follows that above the crest there must be local regions that travel significantly faster.

Thus, mass conservation implies that in the example shown in figure 5, there must be a confined high-speed jet passing over the crest in the antiregular state (cf.

https://doi.org/10.1017/S0022112006009542 Published online by Cambridge University Press

figure 3*a*) inset). This jet is manifested in a localized higher-speed region ($0.5\,\mathrm{m\,s^{-1}}$ indicated) and additionally as this jet enters the slower-moving flow near the trough, it appears to produce a circulatory flow, as shown in the enlarged inset. PIV data here clearly confirm that circulation is present in the antiregular state, whereas we have never witnessed such a circulatory flow in our experiments of the flat or regular states. We remark that the locations of the jet and the presence of circulation are themselves variable: in some PIV experiments, surface eddies are seen and in others they are not. Additionally, it seems likely that the eddies that we saw are a function of the width of our chute, and results may differ in significantly wider (or narrower) chutes. The examples shown in figure 5 were chosen to be representative of typical flows that we observe in our experiments.

To summarize, in the regular state, we see rapid non-circulatory flow that accelerates downstream of the sinusoidal crest and slows upstream. In the antiregular state, we see localized high-speed flows embedded in a slowly moving mass. We also see circulatory flow: this flow is variable, but it seems consistent to surmise that circulation may be generated by strong upstream velocity gradients associated with jets of granular flow over the sinusoidal crest. In the flat flow state, we see nearly uniform velocities that seem consistent with the picture of a sliding layer on a static bed that fills up the sinusoidal troughs. This flow differs qualitatively from the antiregular flow both in asymptotic approach (figure 3*a*) and in that flow in the trough is not static in the antiregular state. This is evidenced from three sources: from external observations through the transparent side of the chute; from PIV data indicating much slower (and therefore thicker) surface flow above the trough in the antiregular state than in the regular; and from transport determinations, discussed next.

Since grains appear to flow and circulate in the troughs of the antiregular state, we are prompted to raise the obvious question: what is going on in the troughs? In the next section, we explore this issue by examining Lagrangian transport of grains through the trough.

5.1. *Transport*

Grains tend to move slowly and irregularly near the sidewalls, and so PIV taken from the side is not revealing; instead we study complex vertical particle motions by freezing the granular bed after releasing alternate streams of red and blue sand down the sinusoidal chute. We perform these experiments as follows. We position the chute at 31.5°, so as to establish antiregular flow (cf. figure 3*a*). We insert a stoppered funnel containing blue sand into the inlet hopper, which we then fill with identical but red sand. This smaller funnel outlet completely blocks the hopper outlet so that no sand flows while the smaller funnel stopper is in place. We initiate flow by pulling the stopper, and when the blue grains are almost exhausted, we rapidly remove the smaller funnel, permitting red grains to flow. We use enough blue grains to fully establish steady antiregular flow, and in this way, we input a uniform flow of grains that abruptly changes from blue to red.

As a first example illustrating the flow dynamics, in figure 6(*a*), we show successive snapshots taken from the side of the chute in the antiregular state. The blue grains have occupied the trough and the red grains are seen to penetrate into the bed from the top as time evolves. In the enlarged views in figures 6(*b*) and 6(*c*), we see that the mechanism of this penetration is that the bed overturns, subducting the red grains in recirculating loops (indicated by arrows). Two such recirculation loops are evident in figure 6(*c*): a downstream loop dominated by blue grains and outlined by a thin strip of red, and an upstream loop dominated by red grains that encircle a central blue

https://doi.org/10.1017/S0022112006009542 Published online by Cambridge University Press

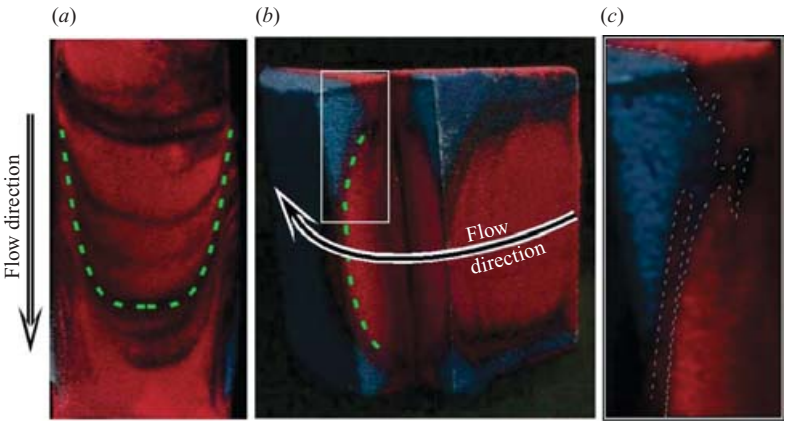


FIGURE 7. (*a*) Snapshot from the bottom of a trough after the flow has been stopped, the bed has been frozen (see text), and the solidified bed has been removed from the chute. Curved 'surrideo' shapes are evident: the dashed curve is the quartic function used in equations (4)–(5). (*b*) Solidified bed removed from the seventh trough downstream. This section of bed has been cut to expose the internal structure. (*c*) Enlarged view of rectangular section from (*b*). Photographic resolution is limited by the size of bed grains, so we identify the approximate red/blue interface with broken lines.

strip of islands. We emphasize that these are not transient effects: the recirculation loops occur in steady, established, flow, and are identifiable only because we have changed the colour of the grains in midstream.

It has been noted in previous work (Shinbrot *et al.* 1999; Taberlet *et al.* 2003; Maneval *et al.* 2005) that granular flows near boundaries often do not faithfully represent interior flows, and so, to reveal the transport internal to the bed, we solidify the bed as follows. First, we stop the flow at a time of our choosing by rapidly bringing the chute to a horizontal position. Inflowing (red) sand then spills over the chute near its inlet, and the grains flowing down the chute stop very rapidly – from observation, the grains seem to stop essentially immediately, and by raising the hinged chute smoothly, no backflow or other spurious effects are evident. After stopping the flow, we solidify the (now horizontal) bed by infiltrating it with a low-viscosity polymeric solution (Rave®, Unilever, Greenwich, CT), and then letting the polymer set over a period of two weeks (Wightman *et al.* 1995). The solidified bed of sand is finally removed, cut and labelled. In figure 7(*b*), we show a representative photograph of the resulting cut section.

The flow patterns produced by this technique are probably not absolutely identical with those that would be seen if the bed could be truly instantaneously frozen in time. Nevertheless, the patterns of flow that we observe seem to reveal faithfully the underlying behaviours that we seek to understand. In particular, as we will describe, patterns of blue and red interfaces develop more detail at successive downstream troughs in a way consistent with the assumption that similar, iterative, circulatory flows (Shinbrot *et al.* 1999; Taberlet *et al.* 2003; Maneval *et al.* 2005) are present in each trough.

Using this solidification technique, in figure 7(*a*) we show a view from the bottom of the bed; this is a snapshot of the solidified mass after it has been lifted off of the sinusoidal supporting plate – the valley of the sine is in the centre of the snapshot, and peaks of the sine are at top and bottom. This particular snapshot is taken from

https://doi.org/10.1017/S0022112006009542 Published online by Cambridge University Press

the third well from the top, shortly after the red grains have fully extended along the length of the chute. In this view, we can identify two features of interest: first, the darker blue grains form multiple striations, suggesting that a repeated sequence of processes has overturned the bed from top (red) to bottom (blue). Second, the striations are significantly curved into 'surrideos' (smile-shapes). We indicate these by green broken lines. This is as we would qualitatively expect for a flow that is nearly stalled near the sidewalls and flows more rapidly toward the chute centreline. We will simulate the apparent velocity field in the next section, and both of these facts will come into play as we construct the simulation.

In another view in figure 7(*b*), we display the contents of a solidified well (the seventh from the top of the chute) that has been sawn open to reveal the internal structure of the bed. The bottom of the well is facing the camera, and one side-surface is visible at the top of the snapshot. From this snapshot, it appears that a rounded bolus of red grains projects into the bed of blue grains, evidently leaving a curved interface in the cross-stream plane. Here again, the wells further down the chute have more interfacial striations than the wells upstream, suggesting that projections form within each well and are convected downstream. The precise details of the process by which projections infiltrate and mix are clearly complex, as indicated in the enlarged view in figure 7(*c*). Here we see that foliated striations (locations approximated by grey broken lines) appear at the interface between red and blue regions, possibly as a result of intermittent stick–slip motion (Shinbrot *et al.* 1999).

5.2. *Velocity fluctuations*

Granular flows tend to be somewhat noisy, and we did not obtain informative data on velocity fluctuations using short-term measurements. Instead, we have characterized temporal velocity fluctuations by comparing successive moving averages from velocimetry data. For each of the flow regimes, we form differences between successive average flows as follows. Using the surface velocimetry data from figure 5, we define the 500-frame (1 s) velocimetry average from frame 1 to frame 500 (within the fourth well from the top of the chute) to be V_1, and the average from frame 501 to frame 1000 to be V_2. We then define the sample velocity fluctuation to be $\Delta V = V_1 – V_2$, which we plot as a function of position within the well in figure 8. We see no significant temporal fluctuations for regular flow, but as shown in figure 8, we do see fluctuations for examples of fully established antiregular and flat flows.

During flat flow (figure 8*a*), fluctuations remain small and broadly distributed, but in each well, the surface does appear to slip uniformly downstream, slow, then slip again. Thus, speed variations in figure 8(*a*) remain small except at the lower section of the trough, where during this slip–slow cycle a slip motion in one well impinges on a slower motion in the next. In antiregular flow (figure 8*b*), by contrast, we see much more dynamic variations in velocity (note scale differences in figure 8). The large peak in the lower region of the trough for this antiregular case corresponds to local increases in speed that are associated with the circulatory flow highlighted in the inset to figure 5.

6. Visualization

The experimental data for regular and flat flows reveal few surprises; regular flow is steady and accelerates with the local slope of the chute bottom, hugging its sinusoidal shape. Flat flow, by contrast, appears to fill in the troughs, and to exhibit a sliding surface layer that slips and slows periodically, but is, by and large, mundane. Antiregular

https://doi.org/10.1017/S0022112006009542 Published online by Cambridge University Press

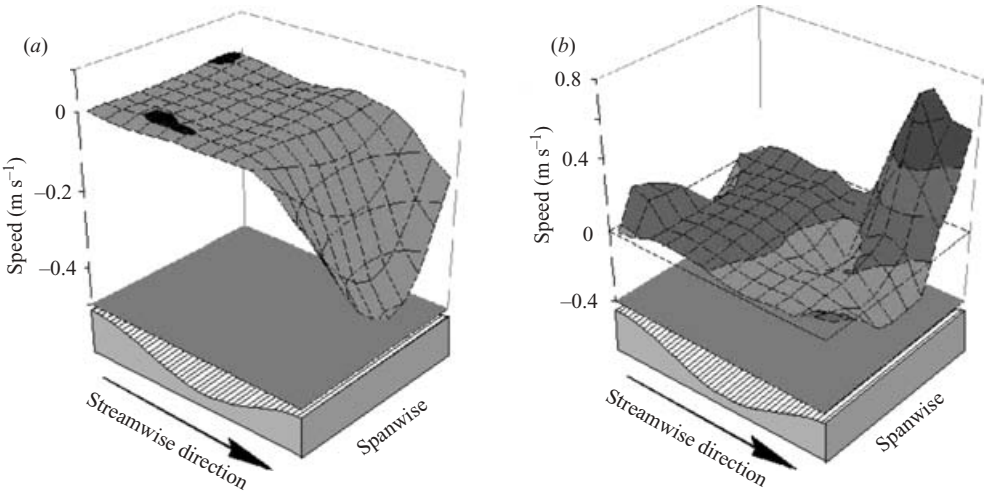


FIGURE 8. Sample velocity fluctuations between two successive seconds of PIV acquisition for: (*a*) flat flow at 30.3° and (*b*) antiregular flow at 31.4°. The highest peak in (*b*) correlates with the presence of a transient circulation region (inset to figure 5) in this particular case.

flow, on the other hand, displays substantial transient accelerations (figure 8*b*) including circulatory flows that sometimes emerge at the surface (figure 5). Averaged over time, transport produces 'surrideo' patterns (figure 7) whose cause is not entirely clear-cut. In this section, we seek to understand better how these patterns are produced. We do this by constructing a Lagrangian flow simulation that permits us to visualize the transport produced by the flow profiles implied by our experimental frozen sections. It is difficult to model accurately granular flows that span kinetics from solid-like to fluid-like (Campbell, Clearly & Hopkins 1995; Gray & Hutter 1997), and so instead, in this simulation, we assume velocity fields that agree with observations and we track markers under the influence of these fields. This is not a first principles simulation; it is merely a visualization method that we use to provide an understanding of how the internal flow seems to behave based on the fixed time snapshots that are attainable.

We generate transport simulations by advecting a plane demarking an imagined interface in the granular bed using the following explicit velocity field, chosen to correspond to data presented in figures 6 and 7:

$$V_x = V_0 \left[\frac{1 + 2(1+z)}{4} + V_2 z|z-1| \right] (1 - V_1 y^4), \tag{4}$$

$$V_z = -V_0 (V_2 x|z-1|)(1 - V_1 y^4). \tag{5}$$

In these equations, $V_{0,1,2}$ are constants (we use $V_0 = V_2 = 0.1$; $V_1 = 0.5$ in figure 9), and the coordinate system is as shown in figure 9(*e*), where x is in the streamwise direction, z is vertical with $z = 1$ at the free surface of the bed. The effects of the separate and combined terms in this velocity field are illustrated in figure 9.

In figure 9(*a*, *b*), we show how the first term in the V_x equation deforms an initial plane of markers. This shear velocity field is chosen after quantitative simulations performed elsewhere (Zheng & Hill 1996; Forterre & Pouliquen 2003). Similarly, in figure 9(*c*), we show how the same initial plane of markers is deformed by the quadratic flow on the right of equation (4), and in figure 9(*d*) we show the combined effects of the shear of figure 9(*b*) and the quartic flow of figure 9(*c*). This quartic field

https://doi.org/10.1017/S0022112006009542 Published online by Cambridge University Press

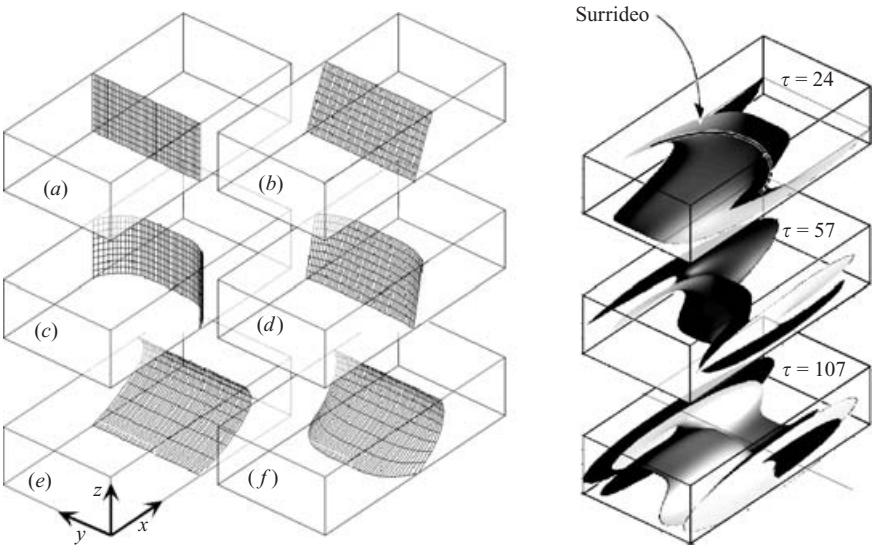


FIGURE 9. Simulated Lagrangian flow used to visualize internal particle motion. (a–f) Illustrations of how an initial plane of markers is transported by the assumed velocity field. (a) Initial plane; (b) first part of assumed velocity: shear produced through drag against the bottom of the chute; (c) second part of the assumed velocity: a quartic profile shown deforming the initial plane of (a); (d) combined effects of shear and quartic flow; (e) combined effects of shear and overturning described in text; (f) combined effects of all of shear, quartic flow and overturning on the initial plane of (a). At the right-hand side is the result of advecting the plane of (a) through 24, 57 and 107 time steps under the combined effects of these flows. The iterated 'surrideo' shape where the curved surface intersects with a horizontal plane is identified at $\tau = 24$; every time the bed turns over, this shape is re-introduced.

is chosen to correspond to the transport data shown in figure 7(a): the green dashed line in this figure is such a quartic. The remaining terms in equations (4) and (5) define a rotation meant to describe the iterative overturning of the bed seen in figure 6.

To illustrate how these flows would deform an initially vertical interface, at the right-hand side of figure 9, we show the shape taken by the initial plane of figure 9(a) after $\tau = 24$, 57 and 107 time steps of Lagrangian transport. At $\tau = 24$, we identify the 'surrideo' shape that is iteratively repeated at later times (not shown to limit clutter). From these Lagrangian transport simulations, we see that each time the bed overturns under the influence of acceleration into and out of successive troughs, a 'surrideo' or smile shape is generated.

7. Conclusion

Our experiments indicate that the bifurcation identified in the nineteenth century for fluid flows over a wavy bottom has a qualitative analogue in granular chute flows. This analogue, however, comes with significant differences in detail. The first of these details is that in the granular case, there are three, rather than only two, distinct states: a flat state at shallow angles of incline; an antiregular state at intermediate angles; and a regular state at the steepest angles. The flat state appears after the trough between successive peaks fills with stalled grains, on which a shallow layer of grains slides nearly uniformly. In this state, kinetic energy appears to be dissipated by slow frictional contacts between the stalled layer beneath and the sliding layer above.

https://doi.org/10.1017/S0022112006009542 Published online by Cambridge University Press

The antiregular state, by contrast, appears from all evidence to be characterized by circulatory flows, which dissipate energy through repeated overturnings of surface layers into the bed. Finally, the regular state exhibits the most rapid mean velocity, with little evidence of mixing, circulation or enduring sliding contacts.

A second major distinction between the fluid and granular transitions is that the fluid transition appears in a solution for inviscid irrotational flow. In the fluid case, regular flow appears at high Froude number and is kinetically driven, while antiregular flow appears at lower Froude number and is driven by a reduction in pressure where the fluid travels rapidly over the peak of a bottom waveform, and an increase in Bernoulli pressure as the fluid travels more slowly over the trough. This causes flow streamlines to converge near the peaks and to diverge near the troughs of the bottom waveform.

By contrast, in the granular case, we know of no simple description that would predict the presence of three distinct flow regimes or that would define the locations of transition boundaries as shown in figure 4. It is dubious whether the Bernoulli equation would ever apply, most notably since sheared grains dilate rather than contract. Moreover, granular flows are strongly dissipative in general, and grains on the wavy bottom are often partially or entirely jammed; additionally, we have shown experimental evidence for significant circulatory flows in the granular case. On all of these accounts, our granular flows are not well described by inviscid or irrotational equations. Nevertheless, there appears to be fortuitous agreement between fluid and granular transitions in flow over a wavy bottom that may give optimism for future hydrodynamic treatments.

Beyond these results of fundamental interest, our results give rise to practical conclusions as well. On the industrial side, our data indicate that either improved bed agitation (in the antiregular state) or complete transport (in the regular state) can potentially be achieved by designing chutes with suitable wavelengths, as informed by figures 3(*b*) and 4(*a*). Additionally, on the geological side, the results suggest that avalanches can display three predictable and distinct regimes of flow, and that by evaluating (or designing) appropriate spacings between natural or artificial obstacles, it may be possible to determine whether avalanches will jet kinetically downslope (for larger spacings on steeper slopes) or overturn in dissipative circulatory loops (for closer spacings). We await corroborating studies as the scale, geometry and materials used are modified.

We thank S. Conway for help with velocimetry measurement, and M. Doumi, N. H. Duong, L. Liwanag and L. Kwan for experimental support. This work was partially supported by the NSF and the ACS-PRF.

REFERENCES

Bagnold, R. A. 1936 The movement of desert sand. *Proc. R. Soc. Lond.* A **157**, 594–620.

Benjamin, E. 1958 Shearing flow over wavy boundary. *J. Fluid Mech.* **6**, 161–205.

Bishop, Lord of Clogher 1713 An account of the subsiding, or sinking down of part of a hill near Clogher in Ireland. *Phil. Trans.* **28**, 267–269.

Bocquet, L., Errami, J. & Lubensky, T. C. 2002 Hydrodynamics model of a dynamical jammed-to-flowing transition in gravity driven granular media. *Phys. Rev. Lett.* **89**, 184301 1–184301 4.

Bridgwater, J. 1976 Fundamental powder mixing mechanisms. *Powder Technol.* **15**, 215–223.

Campbell, C. S., Clearly, P. W. & Hopkins, M. 1995 Large-scale landslide simulations: global deformations, velocities and basal-friction. *J. Geophys. Res.* **100**, 8267.

https://doi.org/10.1017/S0022112006009542 Published online by Cambridge University Press

Denlinger, R. P. & Iverson, R. M. 2001 Flow of variably fluidized granular masses across three-dimensional terrain. 2. Numerical predictions and experimental tests *J. Geophys. Res.* **106**, 553–566.

Dippel, S., Batrouni, G. G. & Wolf, D. E. 1996 Collision-induced friction in the motion of a single particle on a bumpy inclined line. *Phys. Rev.* E **54**, 6845–6846.

Du, Y., Li, H. & Kadanoff, L. P. 1995 Breakdown of hydrodynamics in a one-dimensional system of inelastic particles. *Phys. Rev. Lett.* **74**, 1268–1271.

Forterre, Y. & Pouliquen, O. 2001 Longitudinal vortices in granular flows. *Phys. Rev. Lett.* **86**, 5886–5889.

Forterre, Y. & Pouliquen, O. 2003 Long surface wave instability in dense granular flows *J. Fluid Mech.* **486**, 21–50.

Goddard, J. D. & Alam, M. 1999 Shear-flow and material instabilities in particulate suspensions and granular media. *Particulate Sci. Technol.* **17**, 69–96.

Goldfarb, D., Glasser, B. J. & Shinbrot, T. 2002 Shear instabilities in a granular flow. *Nature* **415**, 302–305.

Goldhirsch, I. & Zanetti, G. 1993 Clustering instability in dissipative gases. *Phys. Rev. Lett.* **70**, 1619–1622.

Gong, W., Taylor, P. A. & Dornbrack, A. 1996 Turbulent boundary-layer flow over fixed aerodynamically rough two-dimensional sinusoidal waves. *J. Fluid Mech.* **312**, 1–37.

Gray, J. M. N. T. & Hutter, K. 1997 Pattern formation in granular avalanches. *Continuum Mech. Thermodyn.* **9**, 675–678.

Gray, J. M. N. T., Tai, Y. C. & Noelle, S. 2003 Shock waves, dead zones and particle-free regions in rapid granular free-surface flows. *J. Fluid Mech* **491**, 161–181.

Günther, A. & Rohr, P. R. V. 2003 Large scale structures in the developed flow over a wavy wall. *J. Fluid Mech.* **478**, 257–285.

Hakonardottir, K. M., Hogg, A. J., Johannesson, T. & Tomasson, G. G. 2003 A laboratory study of the retarding effects of braking mounds on snow avalanches. *J. Glaciol.* **49**, 191–200.

Hanes, D. M. & Walton, O. R. 2000 Simulations and physical measurements of glass spheres flowing down a bumpy incline. *Powder Technol.* **109**, 133–144.

Henrique, C., Aguirre, M. A., Calvo, A., Ippolito, I., Dippel, S., Batrouni, G. G. & Bideau, D. 1998 Energy dissipation and trapping of particles moving on a rough surface. *Phys. Rev.* E **57**, 4743.

Hewgill, D. E., Reeder, J. & Shinbrot M. 1981 Some exact solutions of the nonlinear problem of water waves. *Pac. J. Maths* **92**, 87–109.

Hopkins, W. 1862 On the theory of the motion of glaciers. *Phil. Trans. R. Soc. Lond.* **152**, 677–745.

Howell, D. & Behringer, R. P. 1999 Fluctuations in a 2D granular Couette experiment: a critical transition. *Phys. Rev. Lett.* **82**, 5241–5244.

Hsiau, S. S. & Hunt, M. L. 1993 Shear-induced particle diffusion and longitudinal velocity fluctuations in a granular-flow mixing layer. *J. Fluid Mech.* **251**, 299–313.

Hudson, J. D., Dykhno, L. & Hanratty, T. J. 1996 Turbulence production in flow over a wavy wall. *Exps. Fluids* **20**, 257–267.

Iverson, R. M. 1997 The physics of debris flows. *Rev. Geophys.* **35**, 245–296.

Jaeger, H. M., Nagel, S. R. & Behringer, R. P. 1996 Granular solids, liquids and gases. *Rev. Mod. Phys.* **68**, 1259–1273.

Jenkins, J. T. 1986 *Rapid Flows of Granular Materials.* Cambridge University Press.

Johannesson, T. & Hakonardottir, K. M. 2003 Remarks on the design of avalanche braking mounds based on experiments in 3, 6, 9 and 34 m long chutes. *Vedurstofa Islands Rep.* 03024.

Johnson, P. C., Nott, P. & Jackson, R. 1990 Frictional-collisional equations of motion for particulate flows and their applications to chutes. *J. Fluid Mech.* **210**, 501–535.

Kadanoff, L. P. 1999 Built upon sand: theoretical ideas inspired by granular flows. *Rev. Mod. Phys.* **71**, 434–444.

Komatsu, T. S., Inagaki, S., Nakagawa, N. & Nasuno, S. 2001 Creep motion in a granular pile exhibiting steady surface flow. *Phys. Rev. Lett.* **86**, 1757–1760.

Krettenauer, K. & Schumann, U. 1992 Numerical simulation of turbulent convection over wavy terrain. *J. Fluid Mech.* **237**, 261–299.

Lamb, H. 1932 *Hydrodynamics*, 6th edn. Cambridge University Press.

https://doi.org/10.1017/S0022112006009542 Published online by Cambridge University Press

Losert, W., Bocquet, L., Lubensky, T. C & Gollub, J. P. 2000 Particle dynamics in sheared granular matter. *Phys. Rev. Lett.* **85**, 1428–1431.

Louge, M. Y. 2003 Model for dense granular flows down bumpy inclines. *Phys. Rev.* E **67**, 061303 1–11.

Lyell, C. 1858 On the structure of lavas which have consolidated on steep slopes. *Phil. Trans. R. Soc. Lond.* **148**, 703–786.

Maneval, J. E., Hill, K. M., Smith, B. E., Caprihan, A. & Fukushima, E. 2005 Effects of end-wall friction in rotating cylinder granular flow experiments *Proc. Powders and Grains 2005* (ed. R. Garcia-Rojo, H. J. Herrmann & S. McNamara) Rotterdam.

Menon, N. & Durian, D. J. 1997 Diffusing-wave spectroscopy of dynamics in a three-dimensional granular flow. *Science*. **275**, 1920.

Miller, B., O'Hern, C. & Behringer, R. P. 1996 Stress fluctuations for continuously sheared granular materials. *Phys. Rev. Lett.* **77**, 3110–3113.

Montalbano, E. D. & McCready, M. J. 1998 Laminar channel flow over long and moderate waves. Preprint, Dept. of Chem. Engng University of Notre Dame.

Mueth, D., Debregeas, M. F., Karczmar, G. S., Eng, P. J., Nagel, S. R. & Jaeger, H. M. 2000 Signatures of granular microstructure in dense shear flows. *Nature* **406**, 385–389.

Nakayama, A. & Sakio, K. 2002 Simulation of flows over wavy rough boundaries. *Centre for Turbul. Res. Annu. Res. Briefs*, pp. 313–324.

Pouliquen, O. 1999 Scaling laws in granular flows down rough inclined planes. *Phys. Fluids* **11**, 542–548.

Rabinowicz, E. 1956 Stick and slip. *Sci. Am.* May, 109–116.

Savage, S. B. & Hutter, K. 1989 The motion of a finite mass of granular material down a rough incline. *J. Fluid Mech.* **199**, 177–215.

Savage, S. B., Nedderman, R. M. Tuzun, U. & Houlsby, G. T. 1983 The flow of granular materials – III. *Chem. Engng Sci.* **38**, 189–195.

Shinbrot, T. 1985 A novel model of contact charging. *J. Electrostat.* **17**, 113–123.

Shinbrot, T., Alexander, A. & Muzzio, F. J. 1999 Spontaneous chaotic granular mixing *Nature*. **397**, 675–678.

Silbert, L. E., Ertas, D., Grest,G. S., Halsey, T. C., Levine, D. & Plimpton, S. J. 2001 Granular flow down an inclined plane: Bagnold scaling and rheology. *Phys. Rev.* E **64**, 051302 1–14.

Stoker, J. J. 1957 *Water Waves*, Interscience.

Taberlet, N., Losert, W., Pasini, J. M., Jenkins, J. T. & Delannay, R. 2003 Superstable granular heap in a thin channel. *Phys. Rev. Lett.* **91**, 264301 1–264301 4.

Takahashi, T. 1981 Debris Flow. *Annu. Rev. Fluid Mech.* **13**, 57–77.

Thomson, W. 1886 On stationary waves in flowing water. *Phil. Mag.* **22**, 353–357.

Wightman, C., Mort, R., Muzzio, F. J., Riman, R. E. & Gleason, E. K. 1995 The structure of mixtures of particles generated by time-dependent flows. *Powder Tech.* **84**, 231–240.

Zheng, X. M. & Hill, J. M. 1996 Density and velocity profiles of granular chute flows: a dynamical simulation approach. *Powder Technol.* **86**, 219–228.

https://doi.org/10.1017/S0022112006009542 Published online by Cambridge University Press